This is a preprint of an article submitted to 6th International Conference on Modelling and Simulation for Autonomous Systems held in Palermo, Italy, on 29–30 October 2019. The final version is available under DOI 10.1007/978-3-030-43890-6_11 and online: https://link.springer.com/chapter/10.1007/978-3-030-43890-6_11.

Simulation of UAS-based Radiation Mapping on a Building Surface

Tomas Lazna, Petr Gabrlik, Tomas Jilek, and Frantisek Burian

Central European Institute of Technology, Brno University of Technology, Purkynova 123, 612 00 Brno, Czech Republic
{tomas.lazna,petr.gabrlik,tomas.jilek,frantisek.burian}@ceitec.vutbr.cz

Abstract. This paper is focused on the ionizing radiation intensity mapping to the building surface using an unmanned aircraft system (UAS). The mapping task itself is important for the decommissioning of various nuclear facilities, for example, fuel processing sites or nuclear waste storage areas. The surface map can inform relevant authorities about the strength and distribution of radioactive sources inside. The UAS is exploited for its many advantages, such as low price and a possibility to approach surface closely; moreover, it can acquire a 3D model of the relevant building thanks to, for example, aerial photogrammetry. An approximate model of a real building within our university campus was built with respect to inner structures and classified into several different groups according to construction materials as it is relevant for the simulation of radiation propagation. The choice of the actual study site enables a future experimental verification of proposed methods; in addition, we can work with authentic photogrammetric products obtained during previous flights. Two methods for the surface mapping are suggested and tested on the simulated scenario comprising several radiation sources inside the building. The first technique simply assigns the measured value to the nearest point of the photogrammetric building model, while the other considers also a rough information on the position of sources to estimate the surface intensity more precisely. For better interpretation, scattered data points are interpolated. Finally, the results of both approaches are compared to the computed reference map.

Keywords: Radiation mapping, Simulation, UAS, Aerial photogrammetry

1 Introduction

The radiation mapping is a measurement that provides a knowledge of the radiation distribution in space and time. It can find usage in various areas of men-related activities, such as geophysical survey, first response after nuclear accidents, searching for lost (stolen) sources or general radiation protection. Conservative approach involves helicopter-based systems, however, since the ionizing radiation poses health risks, unmanned assets started to attract attention. Unmanned aircraft systems (UASs) can be used essentially in the same applications with the advantage of lower price and possibility to get to spaces inaccessible to piloted helicopters. After the Fukuschima Dai-ichi Nuclear Power Plant disaster, both an autonomous unmanned helicopter [1] and a UAS [2] were applied to map consequences, i.e., the radiation contamination. The UAS-based mapping took place also in uranium mines [3] to provide data mainly for the radiation protection of tourists.

This paper is focused on radiation mapping of buildings, in other words, it is desired to measure the radiation intensity at their surfaces. Acquired data have a meaning in multiple scenarios: First, the building can be used for industrial or medical procedures that require radiation sources storage and handling, for example, non-destructive testing. In case it is present in an urban area, the mapping should assure the safety of public. Second, the construction can be related to the nuclear technology and utilized for processing or storing radioactive material. It is important to regularly inspect whether there is no leakage of the material. Third, perpetrators may choose the building to hide stolen radiation sources; it is possible to confirm the presence and eventually estimate their location inside the structure. Finally, the construction itself can be made of contaminated building materials. The application of UASs in described tasks is beneficial due to the possibility of approaching the surfaces closely and in a rather fine grid. Consequently, operators are able to build precise surface maps.

We are demonstrating capabilities of the UAS-based surface mapping employing a simulation of radiation measurements. However, the study site is based on a real building located within our campus as we possess its 3D model. Presented methods are designed in a way to be applicable to actually measured data as well. Our team has previous experience with simulating the ionizing radiation, results presented in [4] were later exploited to extend capabilities of a multi-robot system for the localization of radioactive sources described in [5].

The paper is organized as follows. Section 2 provides an overview of methods to simulate the radiation measurements in a vicinity of the studied building. Algorithms for the mapping on surface are introduces in Section 3. Section 4 compiles achieved results and these are summarized and discussed in Section 5.

2 Simulation of Measured Radiation Data

The goal of this portion is to generate radiation intensity data as if they were measured by a UAS flying around a building containing radiation sources. Such simulation must comprise 3D building model including individual materials as they have different attenuation and affects radiation propagation significantly. Based on the intersections of radiation rays with the materials the radiation intensity can be computed for each UAS position and radiation source.

2.1 Radiation Theory

In the scope of this paper, ionizing radiation emitted by radioactive isotope (radionuclide) sources are considered. In most cases, radionuclides decay in alpha or beta mode, yielding heavy or light charged particles respectively. Sometimes, the new isotope remains in excited state and its transition to the base energy is accompanied by the emission of a gamma particle (high-energy photon). As the charged particles interact with an environment more frequently, they have a low penetrability and are unlikely to leave a building, thus, the gamma radiation is studied solely.

A gamma radiation source is characterized by the activity [Bq] which expresses a number of disintegration per second, one or more energy levels of emitted photons [keV] and for each a corresponding yield of photons [%] that states for the portion of emissions per disintegration. Note that the radioactive decay is a stochastic process and the activity represents merely a mean value. The radiation intensity can be represented by, for example, a photon flux of a low practical importance. It is preferable to characterize the radiation intensity by its effect on matter – the dose rate $[\mathrm{Gy} \cdot \mathrm{h}^{-1}]$ embodies a basic quantity that express an increment of the absorbed dose (energy deposited in matter by ionizing radiation per unit mass). For a specific radioisotope of activity A, the dose rate $\dot{D}_1$ present 1 meter away from the source is given by equation [6]:

$$\dot{D}_1 = \frac{\mathit{\Gamma} \cdot A}{3.7 \cdot 10^6} \tag{1}$$

where $\mathit{\Gamma}$ states for the exposure rate constant $[\mathrm{R} \cdot \mathrm{cm}^2 \cdot \mathrm{mCi}^{-1} \cdot \mathrm{h}^{-1}]$ which describes both the energy and the yield of emitted photons.

The propagation of radiation in space is affected by travelled distance and by materials it passes through. The intensity is inversely to proportional to the square of distance (inverse square law). In a material, the radiation exponentially decays with a steepness determined by a linear attenuation coefficient μ which is material-specific and depends on the energy of radiation. When passing through multiple substances, the total attenuation does not depend on their arrangement, overall thickness of each material d is decisive. The propagation of single-energy radiation can be expressed by the following equation:

$$I = I_0 \frac{\exp\left(-\sum_{i=1}^{n} \mu_i d_i\right)}{\left(\sum_{i=1}^{n} d_i\right)^2} \tag{2}$$

where I_0 is the initial intensity.

Ultimately, the photon flux reaches a detection system. Sensitivity of detectors is dependent on the energy of incident radiation and on other factors such as temperature. Moreover, the detection process itself is also stochastic. Let us assume that the detector is well calibrated for the building mapping task and is able to provide correct values of the dose rate in a specified operation range. Then, to make the model simpler, the stochastic character of both the radioactive decay and the detection is included in computation of the dose rate 1 meter away from the source – its value is a random number drawn from the Poisson distribution with the mean value given by equation 1. Due to practical issues, the Poisson distribution is approximated by the Normal one: $\mathcal{P}(\lambda) \sim \mathcal{N}(\lambda; \lambda)$. The distribution remains valid for positive integers, thus, dose rate values are handled in $\mathrm{nGy} \cdot \mathrm{h}^{-1}$.

The radiation emitted by studied sources is not the only one being detected, it is necessary to consider radiation background consisting of two main components: terrestrial and cosmic radiation. The former one is made by radionuclides naturally occurring in our environment (especially the uranium and its decay products such as thorium, radium, etc.) while the other is produced in stars and comes from the outer space. Again, the background level is not a constant value due to the stochastic character of the ionizing radiation origin and detection. We decided to model it by Poisson noise with the mean value $\dot{D}_{Bg}$ provided by, for example, the Safecast project [7].

Given R sources, the dose rate measured by a UAS-based simulated detector can be computed as:

$$\dot{D} = \sum_{r=1}^{R} \frac{(x \leftarrow \mathcal{P}(\dot{D}_{1r})) \cdot \exp\left(-\sum_{i=1}^{n} \mu_{ri} d_{ri}\right)}{\left(\sum_{i=1}^{n} d_{ri}\right)^2} + (y \leftarrow \mathcal{P}(\dot{D}_{Bg})) \tag{3}$$

2.2 Building Model

Three dimensional building model is an essential element for the simulation of the ionizing radiation propagation. Such a model involving individual construction materials and elements may be obtained multiple ways. The most reliable one is to utilize a construction documentation which, besides dimensions and materials, may also includes digital 3D model itself. Another option, chosen by the authors of this work, is to create the model independently. Since we chose a real building situated in the Brno University of Technology campus, we could employ UAS-based photogrammetry for 3D reconstruction. The aerial image data were acquired by the DJI Phantom 3 Advanced UAS, and processed in Agisoft Metashape Professional photogrammetric software previously (Fig. 1). Since we employed position data from low-accuracy onboard global navigation satellite system (GNSS) receiver for georeferencing, the expected absolute model accuracy, considering relevant studies, should be in meter level [8,9]. Such model accuracy, and the average image ground resolution of 1.0 centimeters per pixel, are sufficient values with respect to the discussed application.

The photogrammetry technique, however, reconstructs outer surface only. There are automatic methods, mainly utilized in geographic information system (GIS), which estimate building shapes based on the digital elevation model (DEM, photogrammetric or laser scanning product) [10], however, such techniques also can not reconstruct inner structures. For this reason we used the aforementioned photogrammetry-based model, represented by a point cloud or triangular mesh, and information obtained during actual survey as a basis for manual building digitalization process. A coarse model including inner structures and distinguishing several basic construction materials was assembled in

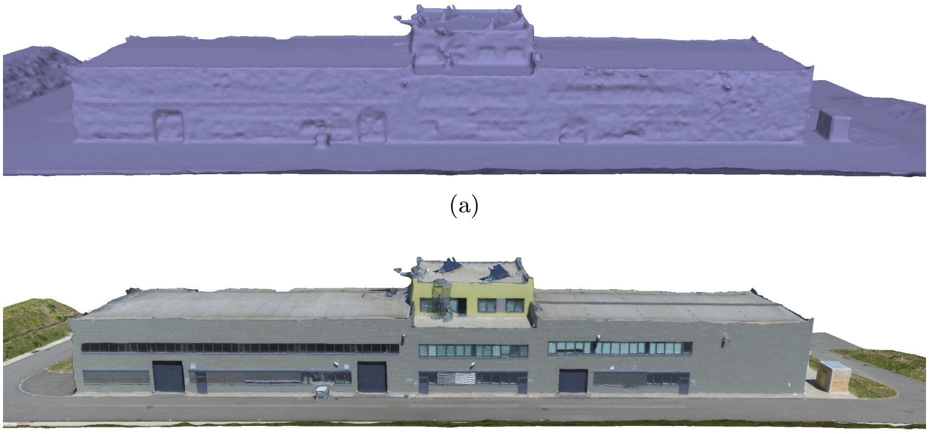

(a)

(b)

Fig. 1: UAS photogrammetry-based 3D model of the actual building (triangular mesh (a), textured mesh (b)).

SketchUp Make 2017 software. For the purpose of the simulation discussed in this paper we consider only the left part of the building illustrated within Fig. 1.

The resultant model, presented in Fig. 2, involves four construction elements represented by different materials: walls, roof, doors and windows. Even though the real building is obviously much more complex, the above-listed elements are most meaningful since they are significantly represented and have different attenuation parameters.

To keep the model adequately straightforward, each construction element is represented by a single material. Walls are modelled by bricks with the attenuation coefficient provided in [11]. Article [12] offers parameters of glass for windows (note that zero concentration of CdO is chosen). In case of doors and the roof, the attenuation is caused especially by plates of aluminium or iron respectively. These objects are therefore perceived as a combination of the metal and thermal isolation where the latter is neglected; relevant parameters of elements can be found in [13]. The idea is to illustrate a difference between building materials rather than to use precise coefficients. Finally, parameters of air are listed in [13] as well. In mentioned references, mass attenuation coefficients are granted; in order to convert them to the linear coefficients they need to be multiplied by the density of relevant material: $\mu = \rho \cdot \mu_m$. Values for the energy of 662 keV are picked as it correspond to selected radiation sources (section 2.4). The elements and material details are summarized within Table 1.

In terms of further processing it is important that every model element is closed (for example every rectangle must have six faces), and individual elements are not overlayed. Finally, the building model is exported as four STL files, one file for each material. This format describes geometry utilizing triangle mesh, each triangle is defined by the coordinates of three vertices.

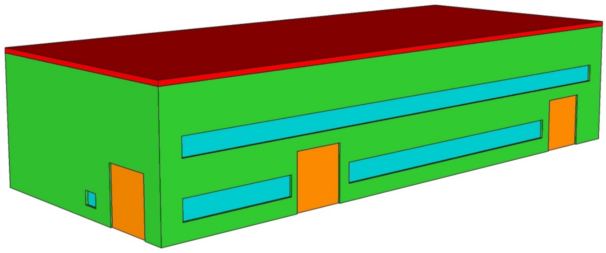

Fig. 2: A coarse digital representation of the left part of the actual building comprising meaningful construction elements and materials: walls (green), roof (red), windows (blue), doors (orange).

Table 1: The construction elements and materials involved in the digitized building model.

Element	Material	Width [m]	μ [cm^{-1}] at 662 keV
Wall	Brick	0.3	0.0567
Roof	Iron (3 %) Therm. isolation (97 %)	0.3	$0.582 \cdot 0.03$
Door	Aluminum (10 %) Therm. isolation (90 %)	0.04	$0.203 \cdot 0.1$
Window	Glass	0.01	0.127
Environment	Air (20 °C)	—	$9.33 \cdot 10^{-5}$

2.3 Analysis of a Material Structure in a Ray Trajectory

Simulation of a measured gamma radiation values by onboard UAS sensor requires the knowledge of a source and UAS position and a total effective thickness of each material that a gamma ray intersect. Structure of materials in gamma ray trajectory can be obtained by analyzing of the sequence of gamma ray intersections with outer surfaces of objects defined by triangle mesh. It is needed to find triangles that gamma ray intersects and the distances between intersections and the source (Fig. 3).

Representation of the building as more separate closed objects allows to analyze an effective thickness of all materials in gamma ray trajectory from a gamma radiation source to a position where a measurement is done. Thickness estimation of all intersected materials is based on sorted intersections by distance between a gamma radiation source and an intersection of gamma ray with triangle that is a part of an outer surface of some object. A ray and triangle intersection is solved via algorithm by Moller and Trumbore [14].

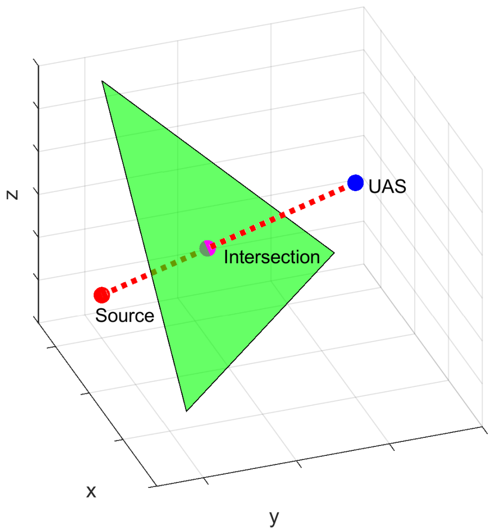

Fig. 3: Gamma ray intersection with triangle.

The estimation algorithm in the first stage detect the first material of a structure as a material of an object in that the gamma source is placed and in the next stage the sorted gamma ray intersections with triangles are analyzed to estimate the type of material that it is in front of the every surface on that the intersection is detected. This approach requires consistent models of building parts; for a valid material estimation it is required to have models without mutual overlap. If the UAS position is outside of the whole model of the building, the material of environment (typically it is air) is added as the last material in the gamma ray trajectory to the estimated structure.

All thicknesses of the same material in the estimated material structure are summed together to get a total material thickness for every crossed material by a gamma ray. Total attenuation of gamma radiation is computed from a partial attenuations caused by all types of crossed materials with their estimated total thickness as it is described by equation 3.

2.4 Experimental Setup

The presented research consider one scenario which involves the following: the building model introduced in section 2.2, UAS trajectory defining positions where the radiation is measured, and several radiation sources located inside the building.

The simulated UAS flight was designed with respect to the flight characteristics of a real unmanned aircraft. Considering our application, where the UAS is

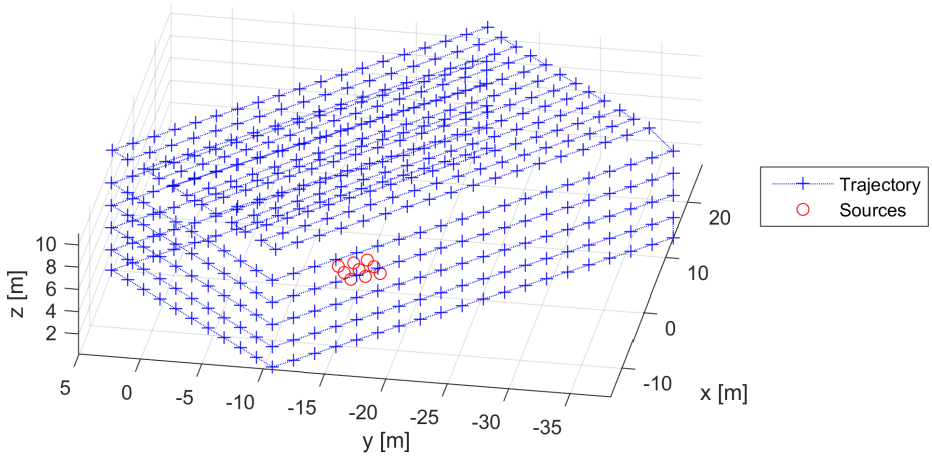

Fig. 4: The UAS trajectory covering the space three meters away from the building surface. The waypoints (blue crosses) correspond the positions, where the radiation is to be measured; nine radiation sources are located inside the building.

intended to fly as close the building surface as possible, the only possibility is to employ a multi-rotor aircraft enabling movements in all directions and hovering. The minimum safe distance from the surface mainly depends on the navigation system accuracy, which is, in the case of consumer-grade GNSS receivers, in meter level. Accordingly, the designed trajectory is three meters away from the building at any moment. Close ground flying, if necessary, can be potentially replaced by unmanned ground vehicle (UGV) deployment [15].

The flight speed of 2 $\mathrm{m \cdot s^{-1}}$, a realistic value chose for the simulation, leads to the measuring interval of 2 meters considering one second sampling period. To cover the building surface homogeneously with a 2×2 m grid, the identical interval was set as the distance between individual flight lines. As a consequence of this setting, the trajectory consists of five layers around the building facade, and one layer over the roof. The situation is illustrated within Fig. 4.

A scenario is assumed in which some perpetrators stole radioactive nuclides and hid them inside warehouse; sources are divided into multiple crates as they were transported from different locations. The setup involves 9 identical unshielded sources deployed in a regular square grid with the area of 6.6 $\mathrm{m^2}$ in the height equal to 0.5 m above ground level (Fig. 4). A rather common radioisotope Caesium-137 was chosen (it is utilized, for example, in radiation therapy or in gamma ray well logging devices); it emits photons with the energy equal to 662 keV with the yield of 85.1 % [16] corresponding to the exposure rate constant of 3.43 $\mathrm{R \cdot cm^2 \cdot mCi^{-1} \cdot h^{-1}}$ [17]. Total activity of sources is equal to 400 MBq – the value was selected with respect to the possibility to detect increased radiation levels outside the building. Average background radiation level in the location equals 110 $\mathrm{nGy \cdot h^{-1}}$.

3 Radiation Mapping Methods

This section explains how to process data either simulated or actually measured in a vicinity of the building. The goal is to acquire a smooth picture of the radiation intensity distribution at surfaces. Two methods to converse 'air' data points to the 'surface' ones are suggested. These points are then interpolated to form the map.

3.1 Radiation Mapping Method 1

The first method is rather straightforward – the dose rate value of a point is assigned to its perpendicular projection on the relevant surface (either a wall or a roof). To find the projection analytically, it would be necessary to divide data points into subsets and provide each one with a corresponding directional information. Instead, a simplification is made and it is assumed that the projection equals the nearest element of a point cloud representing the building model. At lower altitudes, the nearest points are located on ground, therefore, only points having the height greater than a threshold are selected for processing. Due to uneven density of the earlier acquired point cloud especially in its vertical parts (walls), the assumption is not generally valid and there is a chance of assigning multiple values to the same point; in such case, they are averaged.

It is apparent that the accuracy of this approach decreases with the increasing distance from the studied object. Main benefits include simplicity and, above all, the method allows to evaluate results given by the procedure described below.

3.2 Radiation Mapping Method 2

The other method addresses issues linked to the data acquisition relatively far from surfaces via estimating a point in which the radiation originates. Such point does not physically correspond to a specific radiation sources as there are multiple radioisotopes in out scenario; it rather represents a 'center of radiation' (analogy with the center of mass). Knowledge of the center's position can help to compensate errors induced by the measurement geometry if sources are organized in a compact formation.

The estimation itself is based on an initial guess improved by the Gauss-Newton algorithm that is used to solve non-linear least squares problems. Four parameters of the center are sought: its coordinates (x, y, z) and the emitted dose rate $\dot{D}_1$. It minimizes the sum of residuals r_m expressed for individual data points as:

$$r_m = \dot{D}_m - \dot{D}_{EstBg} - \frac{\dot{D}_1}{(x_m - x)^2 + (y_m - y)^2 + (z_m - z)^2}, \tag{4}$$

where triplet (x_m, y_m, z_m) states for the point's coordinates and $\dot{D}_m$ represents measured dose rate and $\dot{D}_{EstBg}$ is the estimated radiation background level. Influence of the attenuation is omitted as the material and structural description

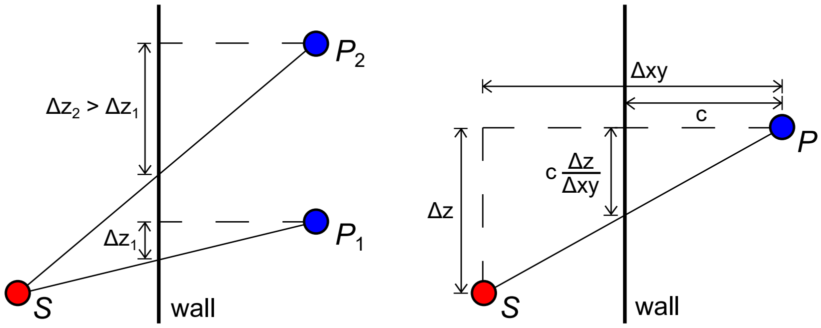

(a) (b)

Fig. 5: The height shift effect (a), and the compensation of the height shift (b); S states for the source position, blue points P_i represent measurement positions.

of the building is generally not available (in this paper, the model is created and used solely for the simulation of measurements). Note that the background needs to be subtracted because it cannot be neglected in comparison with measured values. The proposed model includes only a single virtual source, thus, the result is not overly sensitive to the initial guess: For example, coordinates may be chosen in the building center with the emitted dose rate being equal to the maximal value present in the dataset. The Gauss-Newton method is described by chapter [18] in more detail, its application on a similar problem is then offered in [19].

With the estimated center of radiation, two effects were selected for compensation. First, a measurement point is generally further from sources than its corresponding surface point, therefore, the actual dose rate value present on the surface is greater than the measured one. Second, with the increasing altitudinal difference between sources and a measurement point, the distance of the perpendicular projection and the actual ray intersection is growing (Fig. 5a) causing a height shift of the map. We propose a following solution: To lower measurement altitudes prior to the search for the nearest point and to adjust the dose rate with the ratio of square distances.

Having the point cloud only, the height difference of a measurement point and its corresponding ray intersection cannot be found accurately. Instead, an average value for each flight level is estimated and all relevant points are shifted evenly. The estimation is based on the similarity of triangles (Fig. 5b). After the nearest point (x_s, y_s, z_s) to an adjusted measurement point (x_m, y_m, z_m) with dose rate $\dot{D}_m$ is found, the surface dose rate is computed as:

$$\dot{D}_s = \dot{D}_m \frac{(x_m - x)^2 + (y_m - y)^2 + (z_m - z)^2}{(x_s - x)^2 + (y_s - y)^2 + (z_s - z)^2}. \tag{5}$$

3.3 Data Interpolation

Both described methods yield a set of points with assigned dose rate value – let us denote them as nodes. To build a dense surface map, values in vacant points between nodes need to be interpolated. As the vacant ones, all elements of the point cloud with the minimal distance to nodes being lower that 2 m are selected; the threshold is based on the measurement grid spacing. The interpolation is performed via the MATLAB's `scatteredInterpolant` which is based on the Delaunay triangulation [20].

The resulting interpolated map is used also for the methods accuracy evaluation. First, a reference map is built by computing theoretical values in a regular 0.5 m grid on the surface omitting the stochasticity and the radiation background. Then, to each reference point, the nearest point cloud element is assigned. Finally, a sum of absolute differences between values of corresponding points that exist both in the studied and the reference dataset is computed as the evaluation criterion.

4 Results

The section describes obtained results of measurement simulation and mapping methods for the used building model, radiation sources and a real amount of measurements that are possible to do by on-board radiation sensor. To compare results of different mapping approaches there were simulated reference data on an outer surface of the building. All simulations are processed in MathWorks MATLAB and simulation duration is measured on PC with Intel Core i7-2700K processor.

4.1 Simulated Radiation Data

The models of building parts with their outer surface decomposed to a triangle mesh and simulated positions of data acquisition are shown in Fig. 6. For clarity there are only visualized gamma rays from the first radiation source but the simulation is done for all radiation sources. Applying the algorithm for estimation of a material structure in gamma ray trajectory (described in section 2.3) on all data acquisition positions and all radiation sources positions there is obtained a total attenuation of gamma radiation from every source to every data acquisition position. The result of a material structure analysis for the first radiation source and all positions where the data are acquired is shown in Fig. 7. It is obvious that the material of environment (air) is the most significant component of the material structure in terms of total thickness. In simulation there were used 9 radiation sources and 479 data acquisition points. Triangle mesh describing the building consists of 320 triangles in total (walls: 200, roof: 12, doors: 36, windows: 72). Material structure analysis takes approximately 30 seconds. The reference dataset is acquired by a simulation of measurement in points homogeneously distributed on an outer surface of he building. This dataset consists of

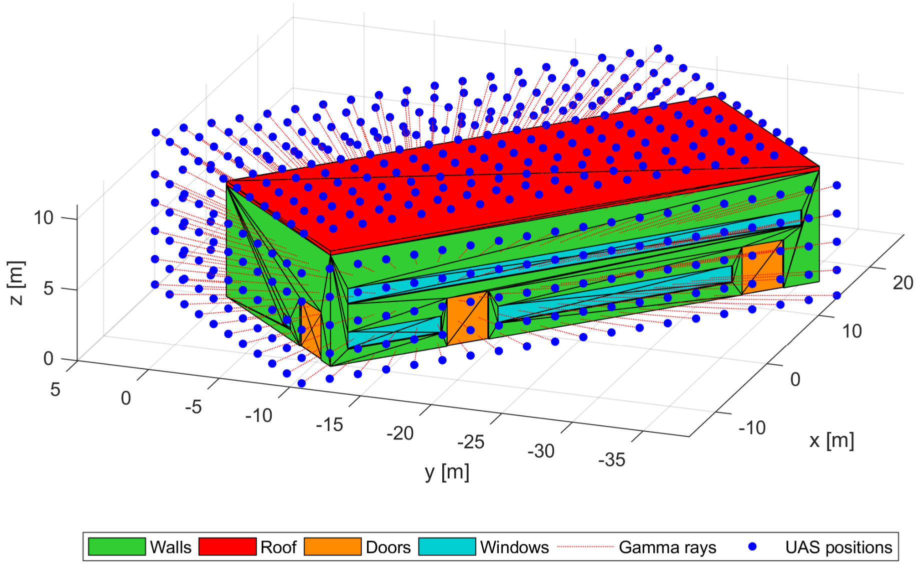

Fig. 6: Models of building parts, simulated data acquisition points and gamma rays from the first radiation source.

5411 points and the simulation takes approximately 6 minutes. The simulated measurements by on-board radiation sensor are visualized in Fig. 8. Computed reference map set into the building point cloud that is based on the simulated radiation measurements on an outer surface of the building is shown in Fig. 9a. Relevant simulation times equal 0.04 s and 0.23 s respectively.

4.2 Radiation Mapping

The described radiation mapping methods were both supplied with the same aforementioned simulated dataset. Both methods took the same total computational time of 5.5 s (the surface mapping: 3 s, the interpolation: 2.5 s). Results are introduced as parts of the photogrammetric building model; they are provided in Fig. 9b and Fig. 9c respectively. The center of radiation was estimated in the position shown in Fig. 10; the distance between the middle source and the center is equal to 0.37 m. The algorithm was provided with the background dose rate of 80 $\mathrm{nGy} \cdot \mathrm{h}^{-1}$; it turned up that the method gives more accurate results when the background is underestimated. In interpolated maps, the door on the longer wall can be clearly seen as the sources were located in their vicinity while the other door on the shorter wall yielded merely an indistinctive spot. Windows can be also partially distinguished in the maps as horizontal stripes of increased dose rate are observable where the glass is. Note that the method 2 assigned the roof greater intensity values in comparison with the reference – that is because

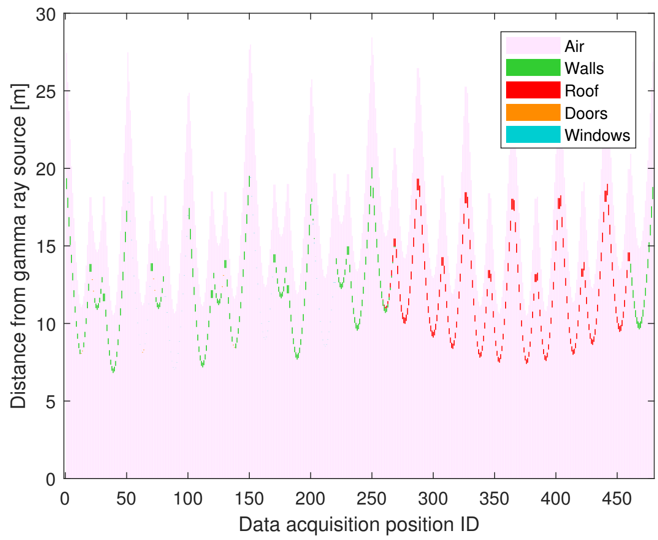

Fig. 7: Estimated structure of materials in gamma ray trajectory for the first gamma source.

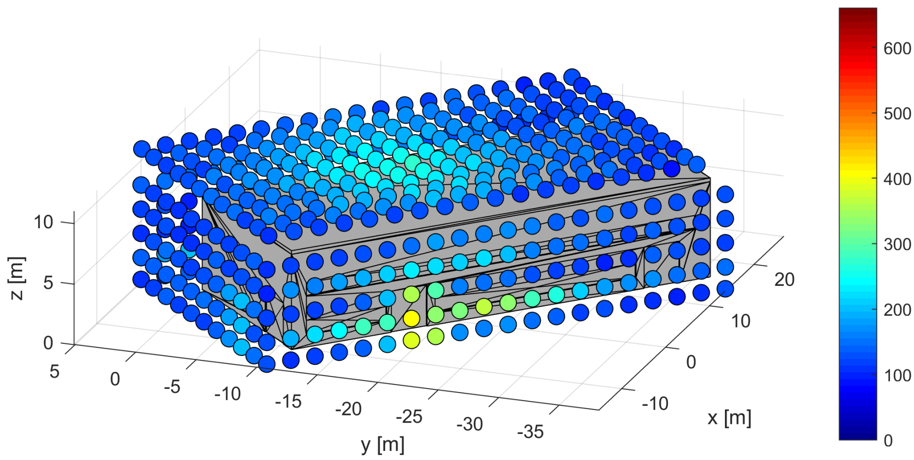

Fig. 8: Visualization of simulated measured values (dose rate in nGy$\cdot$h^{-1}) by on-board radiation sensor.

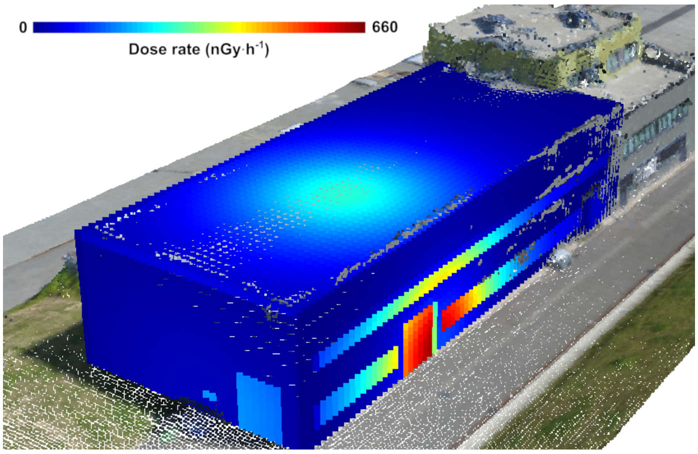

(a)

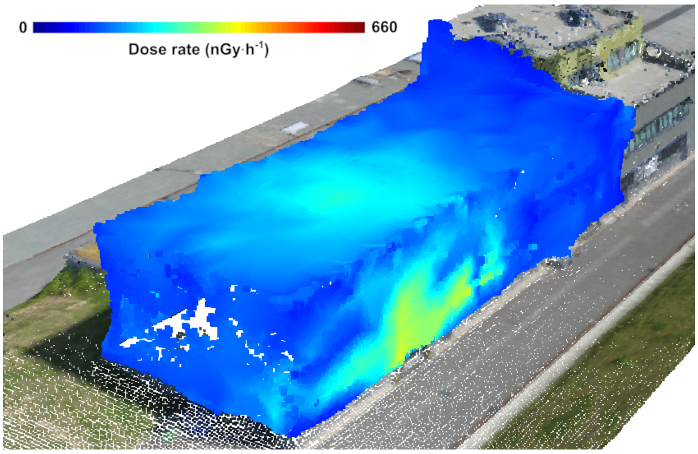

(b)

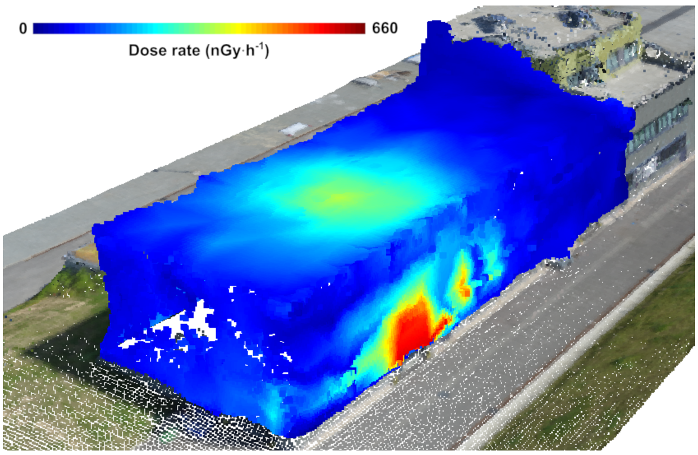

(c)

Fig. 9: Reference surface radiation map (a), and the results of the mapping method 1 (b) and 2 (c) respectively.

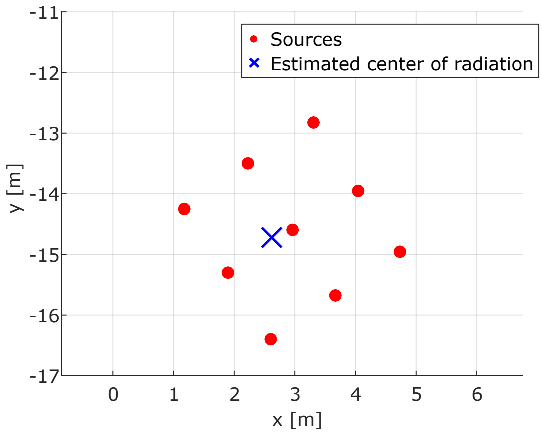

Fig. 10: Estimated center of radiation; the height difference relative to sources equals 0.09 m.

Table 2: Comparison of radiation mapping methods with the reference.

	Sum of errors [nGy·h^{-1}]	Minimum [nGy·h^{-1}]	Maximum [nGy·h^{-1}]	Mean [nGy·h^{-1}]	Stand. dev. [nGy·h^{-1}]
Reference	-	0	635	79	97
Method 1	$4.81 \cdot 10^5$	96	408	161	50
Method 2	$2.92 \cdot 10^5$	6	629	114	90

the roof has actually a strong attenuation which cannot be considered by the designed algorithm.

A numerical comparison with the reference is summarized in Table 2; beside the sum of errors, statistical parameters of all three datasets (namely, minimum, maximum, mean and standard deviation) are offered in order to assess similarity.

5 Conclusion

The aim of this article was primarily to present and compare various methods of radiation intensity mapping to building surface. The analysis was solely performed utilizing simulated radiation data corresponding to a realistic scenario including UAS flight around the actual object. The assembled building model and ray–triangle intersection method allowed us to analyze individual rays trajectories and assess the influence of diverse construction materials. For the simulation, equations describing radiation propagation in the narrow beam geometry were used, although, in fact, the scenario involves the broad beam geometry. This simplification was possible as the distance of both sources and the

UAS from attenuators (obstacles such as walls) was relatively high compared to their thickness and the radiation was monoenergetic.

Both proposed and investigated methods consider the mapping of UAS-measured radiation intensities directly to actual building surface model, which can be acquired via, for example, aerial photogrammetry technique as in our case. We believe this approach preferably highlights the context between the model and radiation levels. The mapping method 1 is very intuitive and straightforward, however, it offers a low level of detail only due to neglecting various effects, such are the actual distance from surface or the source position. More complex method 2 takes into account the measurement geometry, namely, mutual position of sources and data acquisition points. Although the intensity values are altered and do not longer represent the actual local dose rate, the results are significantly better in terms of both details reconstruction and objective assessments. The assembled radiation layer clearly displays construction elements like door, and exhibits a 40 % lower sum of errors from the reference model compared to the method 1. Note that in case the sources were sought as they had been stolen, the algorithm provides their location quite accurately without necessity to enter the building. However, these results were achieved for a rather simplified scenario; it is probable that in a more specific one, the method 2 would not yield such convincing outputs.

Out study still provide wide space for improvements and extension. We would like to focus on multiple experimental setups that are more compelling and compare relevant mapping results. These scenarios may include different types of sources, activities, layouts or different flight trajectories. An improvement of the simulation method could be needed to comprehend other real-world effects, however, we do not have ambition to employ the Monte Carlo N-Particle Transport Code (MCNP) [21] which represents a highly accurate simulation tool as it is not accessible well. In future work, it is also intended to verify developed algorithms experimentally.

Acknowledgments. This work was supported by the European Regional Development Fund under the project Robotics 4 Industry 4.0 (reg. no. CZ.02.1.01 /0.0/0.0/15_003/0000470).

References

1. Sanada, Y., Torii, T.: Aerial radiation monitoring around the Fukushima Dai-ichi nuclear power plant using an unmanned helicopter. J. Environ. Radioact. 139, 294–299 (2015)
2. Martin, P.G., Payton, O.D., Fardoulis, J.S., Richards, D.A., Yamashiki, Y., Scott, T.B.: Low altitude unmanned aerial vehicle for characterising remediation effectiveness following the FDNPP accident. J. Environ. Radioact. 151, 58–63 (2016)
3. Martin, P.G., Payton, O.D., Fardoulis, J.S., Richards, D.A., Scott, T.B.: The use of unmanned aerial systems for the mapping of legacy uranium mines. J. Environ. Radioact. 143, 135–140 (2015)

4. Gabrlik, P., Lazna, T.: Simulation of Gamma Radiation Mapping Using an Unmanned Aerial System. In: 15th IFAC Conference on Programmable Devices and Embedded Systems PDeS 2018, pp. 256–262. Elsevier (2018)
5. Lazna, T., Gabrlik, P., Jilek, T., Zalud, L.: Cooperation between an unmanned aerial vehicle and an unmanned ground vehicle in highly accurate localization of gamma radiation hotspots. Int. J. Adv. Robot. Syst. 15(1), 1–16 (2018)
6. Knoll, G.F.: Radiation Detection and Measurement. John Wiley & Sons, Hoboken, New Jersey (2010)
7. Brown, A., Franken, P., Bonner, S., Dolezal, N., Moross, J.: Safecast: successful citizen-science for radiation measurement and communication after Fukushima. J. Radiol. Prot. 36(2), S82–S101 (2016)
8. Stöcker, C., Nex, F., Koeva, M., Gerke, M.: Quality assessment of combined IMU/GNSS data for direct georeferencing in the context of UAV-based mapping. In: International Conference on Unmanned Aerial Vehicles in Geomatics, pp. 151–157. Bonn, Germany (2017)
9. Lo, C.F., Tsai, M.L., Chiang, K.W., Chu, C.H., Tsai, G.J., Cheng, C.K., El-Sheimy, N., Ayman, H.: The Direct Georeferencing Application and Performance Analysis of Uav Helicopter in Gcp-Free Area. In: International Conference on Unmanned Aerial Vehicles in Geomatics, pp. 151–157. Toronto, Canada (2015)
10. Lafarge, F., Descombes, X., Zerubia, J., Pierrot-Deseilligny, M.: Building reconstruction from a single DEM. In: 2008 IEEE Conference on Computer Vision and Pattern Recognition, pp. 1–8. Anchorage, AK, USA (2008)
11. Salinas, I.C.P., Conti, C.C., Lopes, R.T.: Effective density and mass attenuation coefficient for building material in Brazil. Appl. Radiat. Isotopes. 64, 13–18 (2006)
12. Ahmed, G.S.M., Mahmoud, A.S., Salem, S.M., Abou-Elnasr, T.Z.: Study of Gamma-Ray Attenuation Coefficients of SomeGlasses Containing CdO. Am. J. Phys. Appl. 3(4), 112–120 (2015)
13. Hubbell, J.H., Seltzer, S.M.: Tables of X-Ray Mass Attenuation Coefficients and Mass Energy-Absorption Coefficients. National Institute of Standards and Technology, Gaithersburg, Maryland (2004)
14. Moller, T., Trumbore, B.: Fast, minimum storage ray-triangle intersection. Journal of Graphics Tools. 2(1), 21–28 (1997)
15. Nejdl, L., Kudr, J., Ruttkay-Nedecky, B., Heger, Z., Zima, L., Zalud, L., Krizkova, S., Adam, V., Vaculovicova, M., Kizek, R.: Remote-Controlled Robotic Platform for Electrochemical Determination of Water Contaminated by Heavy Metal Ions. Int. J. Electrochem. Sc. 10(4), 3635–3643 (2015)
16. Be, M.M. et al.: Monographie BIPM-5 – Table of Radionuclides vol. 3. Bureau International des Poids et Mesures, Sevres, France (2006)
17. Smith, D.S., Stabin, M.G.: Exposure Rate Constants and Lead Shielding Values For Over 1,100 Radionuclides. Health Phys. 102(3), 271–291 (2012)
18. Deuflhard, P.: Least Squares Problems: Gauss-Newton Methods. In: Newton Methods for Nonlinear Problems, Springer Series in Computational Mathematics, pp. 173–231. Springer, Heidelberg (2011)
19. Lazna, T.: Optimizing the localization of gamma radiation point sources using a UGV. In: 2018 ELEKTRO. IEEE (2018)
20. Amidror, I.: Scattered data interpolation methods for electronic imaging systems: a survey. J. Electron. Imaging. 11(2), 157–176 (2002)
21. Goorley, T. et al.: Features of MCNP6. In: SNA + MC 2013 - Joint International Conference on Supercomputing in Nuclear Applications + Monte Carlo. EDP Sciences, Les Ulis, France (2014).